# Phosphorescence and Optically Detected Magnetic Resonance of 4′,6-Diamidino-2-phenylindole (DAPI) and Its Complexes with $[d(CGACGTCG)]_2$ and $[d(GGCCAATTGG)]_2$†

Ajay Misra, Andrzej Ozarowski, and August H. Maki*

*Department of Chemistry, University of California, Davis, California 95616*

*Received February 12, 2002; Revised Manuscript Received March 16, 2002*

ABSTRACT: Phosphorescence and optical detection of magnetic resonance (ODMR) is used to study the excited triplet state of 4′,6-diamidino-2-phenyl indole (DAPI) and its complexes with the oligonucleotides $[d(CGACGTCG)]_2$ and $[d(GGCCAATTGG)]_2$, where binding occurs by intercalation between GC base pairs and by minor groove insertion, respectively. Weaker binding of DAPI to phosphate is also detected, and the triplet state of this complex is characterized. Intercalation with $[d(CGACGTCG)]_2$ produces a phosphorescence redshift, while groove binding with $[d(GGCCAATTGG)]_2$ leads to a blueshift. Both binding modes give rise to a small decrease in the zero-field splitting (zfs) of the DAPI triplet state. The largest redshift and zfs decrease are found for the phosphate complex. The phosphorescence lifetimes are shorter by an order of magnitude than that of indole or tryptophan as expected for the lower triplet state energy, $E_{00}$, of DAPI. The lifetimes agree well with a correlation with $E_{00}$ introduced by Siebrand [Siebrand, W. (1966) *J. Chem. Phys. 44*, 4055−4057] except for the $[d(GGCCAATTGG)]_2$ minor groove complex with a lifetime that is about 20% too long. The longer lifetime is attributed to distortion of the amidino groups in this complex, resulting in less efficient intersystem crossing.

A great deal of interest has been focused on drugs that exert their biological effects by forming complexes with nucleic acids (*1*, *2*). Two primary drug-binding modes have been recognized, intercalation and minor groove interactions. The former is represented by planar fused aromatic cations, such as quinacrine and ethidium (*3*, *4*). Minor groove-binding drugs, on the other hand, are represented by nonfused cations such as netropsin and distamycin (*5*). These are selective for AT sequences, to avoid contact with the bulky $NH_2$ group of CG base pairs at the foot of the minor groove or because of favorable electrostatic interactions with the negatively charged minor groove in A·T sequences (*6*). 4′6-Diamidino-2-phenylindole (DAPI, Figure 1)[1] is an aromatic diamidine having antitrypanosomal (*7*), antibiotic, antiviral, and antitumor activity. By inhibiting the binding of essential enzymes to duplex DNA, it alters biomolecular processes such as replication, repair, and transcription (*8*−*10*). DAPI finds wide use as a DNA probe in cytological applications, owing to the large increase in its fluorescence quantum yield on binding to duplex DNA (*11*−*13*). DAPI has the properties of a minor groove-binding drug, and this binding mode has been characterized in AT sequences of DNA (*5*, *11*, *14*, *15*).

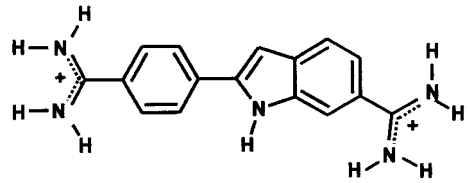

FIGURE 1: Structure of the dication of DAPI.

However, intercalation of DAPI occurs in CG sequences (*16*, *17*), and stacking with terminal CG base pairs also has been recognized (*18*). Additionally, intercalation at AU sites of duplex RNA is found, in contrast with the minor groove binding at AT sites of DNA (*19*).

In this paper, we employ low-temperature phosphorescence and optically detected magnetic resonance (ODMR) spectroscopy to study DAPI and two of its DNA complexes that have been characterized previously by other methods, the complex with $[d(CGACGTCG)]_2$ and the complex with $[d(GGCCAATTGG)]_2$. The binding of DAPI to the octanucleotide duplex $[d(CGACGTCG)]_2$ has been studied by NMR (*17*) and reveals the presence of two nonequivalent binding sites formed by intercalation of the drug into the central adjacent CG base pairs and into the terminal adjacent CG base pairs. Crystals of the complex of DAPI with $[d(GGCCAATTGG)]_2$ have been studied by X-ray diffraction (*20*) showing that the drug binds into the minor groove formed by the central AT base pairs. In this work, we utilize the influence of the local environment on the triplet state properties of DAPI as revealed by phosphorescence and ODMR spectroscopy to distinguish between and characterize the two primary binding modes of this drug, minor groove binding and intercalation. Additionally, the binding of DAPI

† This publication was made possible by Grant No. ES-02662 from the National Institute of Environmental Health Sciences. Its contents are solely the responsibility of the authors and do not necessarily reflect the views of NIEHS, NIH.

* To whom correspondence should be addressed. Phone: (530) 752-6471; Fax: (530) 752-8995; E-mail: maki@indigo.ucdavis.edu.

[1] Abbreviations: *D* and *E*, zero-field splitting parameters; DAPI, 4′,6-diamidino-2-phenyl indole; EEDOR, electron−electron double resonance; EG, ethylene glycol; MIDP, microwave-induced delayed phosphorescence; ODMR, optically detected magnetic resonance; SLR, spin−lattice relaxation; zfs, zero-field splitting.

10.1021/bi020124j CCC: $22.00 
Published on Web 04/27/2002

to phosphate is detected, and the adduct is characterized by its phosphorescence and ODMR spectra. These methods have been used previously to study the triplet state of tryptophan in various proteins sites and in protein−nucleic acid complexes (*21*−*23*).

## MATERIALS AND METHODS

DAPI dihydrochloride dihydrate was purchased from Sigma and used without further purification. The oligonucleotides were synthesized by the Molecular Structure Laboratory, University of California, Davis. DAPI (0.2 mM) and the oligonucleotides (0.4 mM) are dissolved in 10 mM phosphate buffer, pH 7. Complexes are prepared by mixing equal volumes of DAPI and DNA monomer solutions to form a 1:1 DAPI dsDNA complex. After 1 h, 40 vol % of ethylene glycol (EG) is added as cryosolvent and aliquots of 40 $\mu$L are introduced into 2 mm inside diameter Spectrasil tubes for low-temperature spectroscopic measurements. To assess the effects of pH and buffer concentration on the spectra of DAPI, 40% EG-containing samples are made up with water, $10^{-2}$ M HCl, $10^{-2}$ M NaOH, and pH 7 phosphate buffer at 2 mM and 100 mM concentration.

Phosphorescence measurements are made at 77 and 4.2 K with the sample excited by the 365 nm band of a 100 W high-pressure Hg arc lamp that is selected by a 0.1 m monochromator with 16 nm bandwidth. Only DAPI is excited at this wavelength in DNA complexes. The phosphorescence is observed through a 1 m monochromator using 3.2 nm bandwidth.

ODMR experiments are carried out at 1.2 K in pumped liquid He in order to minimize spin−lattice relaxion (SLR). The spectrometer, employing photon counting, has been described previously (*24*, *25*). ODMR center band frequency $\nu_0$ and bandwidth $\nu_{1/2}$ (half height at half-maximum intensity (hwhm)) are obtained using the delayed slow-passage experiment, as described previously (*26*, *27*).

The energies of the triplet state sublevels are given in zero magnetic field by the eigenvalues of the spin Hamiltonian (*28*)

$$\mathcal{H}_s/h = D(\mathcal{S}_z^2 - {}^2/_3) + E(\mathcal{S}_x^2 - \mathcal{S}_y^2)$$

where $D$ and $E$ are the triplet state zero-field spitting (zfs) parameters, $\mathcal{S}_i$, $i = x, y, z$ are the spin operators, and $h$ is Planck's constant. The energies of the sublevels, $T_z$, $T_y$, and $T_x$ are $-{}^2/_3Dh$, $({}^1/_3D + E)h$, and $({}^1/_3D - E)h$, respectively. Taking $z$ as the out-of plane principal axis, $D > 0$ for $^3(\pi, \pi^*)$ states of aromatic molecules, such as indole and DAPI. Furthermore, we arbitrarily adopt the convention $E > 0$ without specifying the directions of the in-plane $x$- and $y$-principal axes. With this convention, the energies ($\epsilon_i$) of the sublevels increase in the order $\epsilon_z < \epsilon_x < \epsilon_y$. For indole, the principal $x$ axis is approximately normal to the ethylenic bond of the five-membered ring (*29*).

For DAPI, and its complexes with DNA, we find that $D \sim 3E$ (see the following discussion). Thus, the $D - E(T_x \leftrightarrow T_z)$ and the $2E(T_x \leftrightarrow T_y)$ ODMR bands overlap. Because the $T_x$ and $T_y$ sublevel populations decay rapidly relative to that of $T_z$ (see the following discussion), the $2E$ band vanishes shortly after the excitation is terminated. Thus, when employing delayed ODMR, only the $D - E$ and $D + E$ bands are found, and these are used to obtain the zfs parameters.

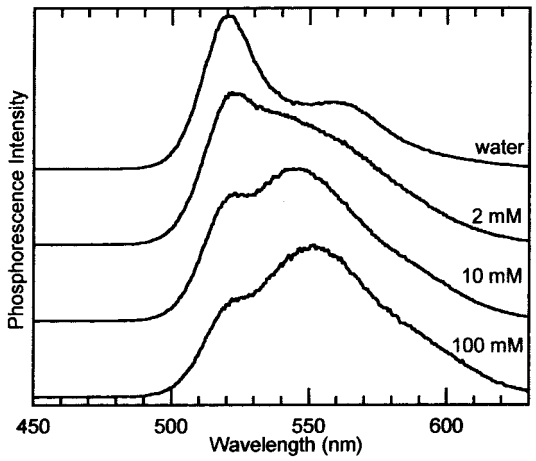


FIGURE 2: Phosphorescence spectra of DAPI in EG−water glass and EG−pH 7 phosphate buffer glass at various phosphate concentrations. The phosphate buffer samples are at 77 K, while the water sample is at 4.2 K. The spectrum of DAPI in water is unchanged at 77 K. Excitation is at 365 nm.

In some samples, both the $D - E$ and the $2E$ bands are observed as a poorly resolved doublet by delayed slow-passage ODMR during saturation of the $D + E$ band (electron−electron double resonance (EEDOR)).

Sublevel decay constants, $k_i$, relative radiative rate constants, $r_{ix} = k_i^r/k_x^r$, the SLR rate constants, $W_{ij}$, and the relative initial sublevel populations, $n_{ix}^0 = n_i(t = 0)/n_x(t = 0)$, are obtained from global analysis (*25*) of microwave-induced delayed phosphorescence (MIDP) data sets (*30*). Rapid passage through the $D + E$ band produces a simple transient that is analyzed as a single transition, as described previously (*25*). Rapid passage through the $D - E$, $2E$ frequency region produces a complex response that is analyzed as sequential passages through these bands. The temporal separation of the fast passage responses (assumed instantaneous) is calculated from the microwave sweep rate employed in the MIDP measurement and the frequency separation of the bands that is obtained from analysis of the delayed slow-passage ODMR data.

## EXPERIMENTAL RESULTS

*Phosphorescence Spectra.* The phosphorescence spectra of DAPI in EG glass from water and from various concentrations of pH 7 phosphate buffer are shown in Figure 2. The spectra of DAPI in aqueous EG glass made from 10 mM NaOH and from 10 mM HCl (not shown) resemble closely that of the sample made up in pure water, showing that there is no noticeable effect of acidity on the phosphorescence of DAPI in this pH range and that the effect of buffer concentration is not a general effect of ionic strength but rather is the result of binding of DAPI with phosphate. The narrow band of the free DAPI phosphorescence spectrum that is found at 521 nm diminishes in intensity with increasing phosphate buffer concentration, while a broader peak at 547 nm grows in. The phosphorescence decay kinetics of DAPI in 10 mM phosphate−EG glass differ when monitored at 521 and at 547 nm. At 4.2 K, the decay constant at 521 nm is 1.26 $s^{-1}$, while at 547 nm, the decay is more rapid but cannot be fitted to a single exponential. The band at 547 nm is assigned to the triplet state of a phosphate complex of DAPI. It has widely different properties as

Table 1: Triplet State Spectroscopic Properties of DAPI and Its Complexes with $[d(CGACGTCG)]_2$ and $[d(GGCCAATTGG)]_2$[a]

| sample[b] | $\lambda_{max}$[c] (nm) | $D-E$ | | $D+E$ | | $D$ (GHz) | E (GHz) |
|---|---|---|---|---|---|---|---|
| | | $\nu_0$ (GHz) | $\nu_{1/2}$ (MHz) | $\nu_0$ (GHz) | $\nu_{1/2}$ (MHz) | | |
| DAPI | 521.5 | 1.488(1) | 59(4) | 3.082(2) | 58(4) | 2.285 | 0.797 |
| DAPI | 547 | 1.413(9) | 68(2) | 2.86(1) | 101(23) | 2.13 | 0.72 |
| DAPI + $[d(CGACGTCG)]_2$ | 527 | 1.463(1) | 56(4) | 3.019(5) | 56(7) | 2.241 | 0.778 |
| DAPI + $[d(GGCCAATTGG)]_2$ | 516.6 | 1.464(2) | 50(1) | 3.059(5) | 47(8) | 2.261 | 0.799 |
| DAPI in 10 mM NaOH−EG glass | 521 | 1.492(2) | 56(3) | 3.083(1) | 47(9) | 2.287 | 0.796 |
| DAPI in 10 mM HCl−EG glass | 522 | 1.485(3) | 55(1) | 3.069(5) | 57(2) | 2.277 | 0.792 |
| DAPI in 10 mM HCl−EG glass[d] | 564 | 1.477(9) | 65(6) | 3.064(9) | 65(20) | 2.271 | 0.793 |

[a] Standard deviations in the last digit are given in brackets. [b] Samples are in 40% EG−10 mM pH 7 phosphate glass except as noted. [c] Monitored wavelength; maximum of the high energy band except as noted. [d] Monitored at maximum of the low energy band.

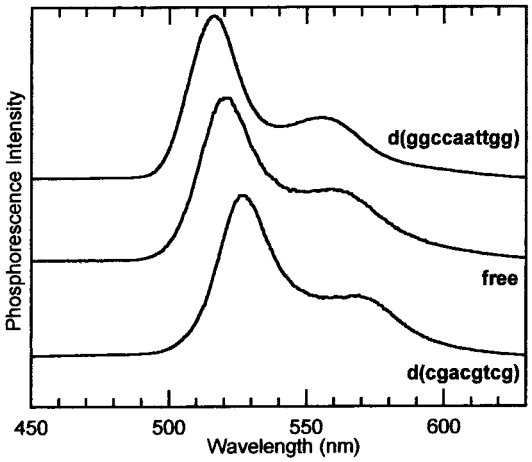


FIGURE 3: Phosphorescence spectra of complexes of DAPI with $[d(GGCCAATTGG)]_2$ and $[d(CGACGTCG)]_2$ compared with free DAPI in EG−water. The oligonucleotide samples are dissolved in EG−10 mM pH 7 phosphate buffer. The oligonucleotide samples are measured at 77 K; the free DAPI is at 4.2 K. Excitation is at 365 nm.

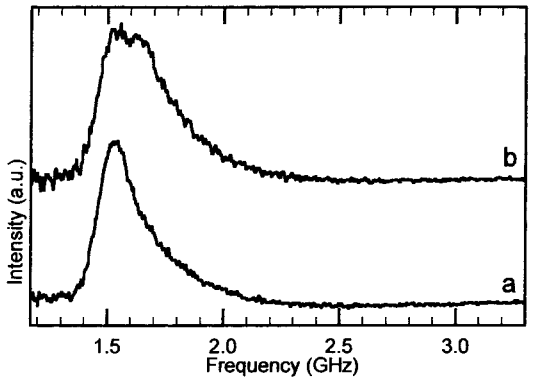


FIGURE 4: Delayed slow-passage ODMR spectra of the DAPI−$[d(GGCCAATTGG)]_2$ complex in the $D-E$ and $2E$ transition region (a) without and (b) with simultaneous saturation of the $D+E$ band. The free decay is subtracted. The sample is at 1.2 K with the phosphorescence monitored at 517.4 nm with 3.2 nm bandwidth. The sample is excited for 5 s. Microwaves are swept between 1.2 and 2.3 GHz in 2.5 s following a free decay interval of 1 s.

revealed by ODMR (see the following discussion). In order to isolate the decay of the phosphate complex, the spectrum of DAPI in EG−water (Figure 2) is subtracted by computer from the spectrum in 10 mM phosphate to produce a spectrum that lacks the peak at 521 nm. The single-exponential decay that is measured at 521 nm is weighted by the contribution of the subtracted spectrum to the total spectrum at 547 nm, and this is subtracted from the observed decay. The remainder is taken as the decay of the phosphate complex and can be fitted to a single-exponential having a decay constant of 1.85 $s^{-1}$.

The phosphorescence of buffer-free DAPI is compared with that of the complexes with $[d(GGCCAATTGG)]_2$ and $[d(CGACGTCG)]_2$ in Figure 3. The spectra have similar contours but differ in the location of the origin band, which is shifted to the blue in the $[d(GGCCAATTGG)]_2$ complex and to the red in the $[d(CGACGTCG)]_2$ complex. The DNA complexes are made up in 10 mM phosphate buffer yet show no trace of the characteristic 547 nm band of the phosphate complex of DAPI (Figure 2), indicating that the phosphate complex is considerably weaker than either DNA complex. The peak wavelengths of the origin band of DAPI and its complexes are given in Table 1.

*Delayed Slow-Passage ODMR Spectra.* A typical delayed slow-passage ODMR spectrum showing the $D-E$ band of the $[d(GGCCAATTGG)]_2$ complex of DAPI is shown in Figure 4. Also shown is the delayed ODMR response in this same frequency range with simultaneous saturation of the $D+E$ band at 3.06 GHz (EEDOR). The emergence of the $2E$ band as a result of EEDOR is clearly visible, displaced to a higher frequency than the $D-E$ band by 140 MHz. Similar results are obtained with the other samples, but the splitting is less and the doublet structure is not sufficiently distinct to allow analysis in terms of two distinct transitions. Thus, the EEDOR spectra are not used, and our analysis is made using only the $D-E$ and $D+E$ bands. The delayed slow-passage ODMR data are given in Table 1, which also lists the $D$ and $E$ parameters for DAPI and its complexes with phosphate and $[d(CGACGTCG)]_2$. The ODMR spectra of DAPI in 10 mM NaOH−EG glass and in 10 mM HCl−EG glass (Table 1) are unchanged from those of DAPI in 10 mM phosphate buffer monitored on the blueshifted maximum (521.5 nm). This shows that the triplet state is unaffected by pH in the range represented by these samples. The ODMR of DAPI in phosphate buffer monitored at the redshifted maximum (547 nm) differs considerably from these and is assigned to a phosphate complex.

*Triplet State Kinetics from MIDP.* The MIDP data sets for the DAPI complex of $[d(GGCCAATTGG)]_2$ in 10 mM phosphate buffer are shown in Figure 5. The data for the $D+E$ transition (lower data set) are normal, because only a single band is saturated, but the complex form of the other data set is obvious, because two transitions, the $D-E$ and then the $2E$ band, are traversed sequentially. The nature of the response is readily understood if we assume, for the moment, the following scheme (verified by global analysis of the MIDP data; see the following discussion). The populations of the $T_x$ and $T_y$ sublevels decay rapidly (relative

Table 2: Kinetic and Radiative Parameters of DAPI and Its Complexes with $[d(CGACGTCG)]_2$ and $[d(GGCCAATTGG)]_2$[a]

| sample[b] | $k_{av}$[c] | $k_x$ ($s^{-1}$) | $k_y$ ($s^{-1}$) | $k_z$ ($s^{-1}$) | $r_{zx}$ | $r_{yx}$ | $W_{xy}$ ($s^{-1}$) | $W_{xz}$ ($s^{-1}$) | $W_{yz}$ ($s^{-1}$) | $n_{xx}^0$ | $n_{yx}^0$ | $n_{zx}^0$ |
|---|---|---|---|---|---|---|---|---|---|---|---|---|
| DAPI (521.5 nm) | 1.27 | 1.93(2) | 1.70(2) | 0.15(2) | 0.052(8) | 0.329(7) | 0.00(1) | 0.12(2) | 0.15(1) | 1 | 1.18 | 1.00 |
| DAPI (547 nm) | 1.85[d] | | | | | | | | | 1 | | |
| DAPI + $[d(CGACGTCG)]_2$ (527 nm) | 1.33 | 1.99(1) | 1.68(1) | 0.30(1) | 0.100(6) | 0.325(5) | 0.000(9) | 0.03(1) | 0.000(6) | 1 | 1.22 | 0.90 |
| DAPI + $[d(GGCCAATTGG)]_2$ (516.6 nm) | 0.88 | 1.47(1) | 1.12(1) | 0.036(8) | 0.010(4) | 0.167(4) | 0.094(6) | 0.218(9) | 0.140(6) | 1 | 0.93 | 0.89 |

[a] Standard deviations in the last digit are given in brackets. [b] Monitored wavelength is given in brackets. Sample is in 40% EG−10 mM pH 7 phosphate buffer glass. [c] Decay constant, $s^{-1}$, measured at 4.2 K. [d] Obtained by deconvolution of nonexponential decay. See text.

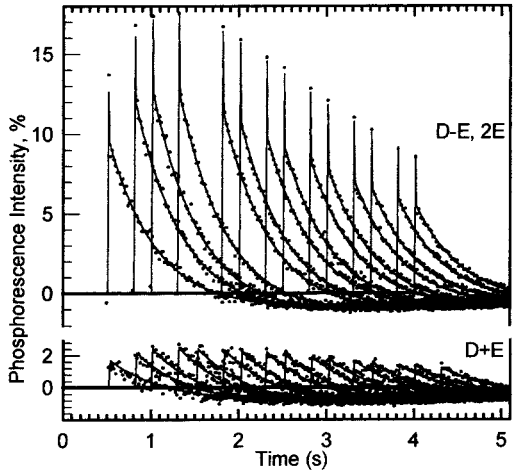


FIGURE 5: MIDP signals of the DAPI−$[d(GGCCAATTGG)]_2$ complex observed in the $D - E$ and $2E$ transition region (above), and in the $D + E$ transition (below). Sample conditions are as given in the Figure 4 caption. The microwave sweep rate through the bands is 20 GHz/s. The sample is excited for 5 s, and each response is averaged 20 times. The solid lines are least-squares fittings of the data set by global analysis (*25*) that produced the kinetic and radiative parameters listed in Table 2.

to the $T_z$ population) after shuttering the excitation light. During the sweep (upward) of the microwave frequency, the $D - E$ band is encountered first, transferring excess population from $T_z$ to $T_x$, which is more radiative than $T_z$. This results in the initial positive phosphorescence transient. When the $2E$ band is encountered subsequently, the excess $T_x$ population is transferred to $T_y$, which is less radiative than $T_x$, resulting in a negative transient followed by normal decay of the phosphorescence. The resulting "spike" has a width of 7 ms or only about two channels in the multichannel analyzer. Yet, it is easily seen and accurately fitted (Figure 5) using a slight modification of the global analysis program (*25*) to account for the two rapid passage events in one of the data sets. The kinetic parameters obtained for DAPI and its oligonucleotide complexes are presented in Table 2.

## DISCUSSION

*Phosphorescence and zfs.* The phosphorescence spectrum of DAPI is found at a much lower energy than that of indole (0,0 band at 403.5 nm in EG−water glass (*31*)), suggesting significant expansion of the electron density onto the 6-amidinium and 2-phenyl-4′-amidinium groups. Significant delocalization of spin density is suggested also by the large reduction in the zfs parameters of DAPI; $D = 3.03$ GHz, $E = 1.28$ GHz for indole (*31*). The unusually large value of $E$ for indole is the result of the concentration of significant electronic density in the ethylenic double bond of the five-membered ring in the triplet state (*32*). The $E/D$ ratio of tryptophan is sensitive to the nature and position of substituents on the indole ring. Substitution of F or $CH_3$ groups in position 6 of indole leads to an increase of $E/D$, while in position 5, these groups as well as OH produce a decrease of this ratio (*26*, *33*). These substitutions lead to only minor changes in $D$, indicating that they do not produce significant delocalization but rather that they cause changes in the spin density in the 2−3 double bond of indole. The smaller value of $E/D$ in DAPI relative to indole, on the other hand, may be a consequence of electron delocalization caused by the 6-amidinium and 2-phenyl-4′-amidinium substituents. Binding of DAPI with phosphate induces a broadening and a redshift of the phosphorescence that peaks at 547 nm (Figure 2). When monitored on this redshifted peak, the ODMR has significantly reduced zfs parameters relative to free DAPI, monitored at 521.5 nm (Table 1). Both the redshift and decreased zfs parameters of the triplet state indicate that a complex is formed with phosphate and suggest that there is increased delocalization of the spin density onto the side groups of indole. Phosphate appears to interact specifically because other anions such as $Cl^-$ and $OH^-$ at 10 mM concentration have no effect on DAPI phosphorescence. It should be noted that, in the absence of phosphate binding, we find the same zfs parameters whether the phosphorescence is monitored on the origin peak at 522 nm or on the redshifted peak at 564 nm (Table 1). Thus, the redshifted peak in free DAPI, $\Delta\omega = 1750$ $cm^{-1}$, results from the vibronic structure of a single triplet state.

Binding of DAPI with $[d(GGCCAATTGG)]_2$ into the minor groove (*20*) leads to a blueshift of the phosphorescence and a small reduction of the zfs relative to free DAPI. The binding of DAPI with $[d(CGACGTCG)]_2$, where it intercalates between GC base pairs (*17*), leads to a redshift of the phosphorescence and a somewhat larger reduction of the zfs. Analogous effects have been noted for tryptophan and are attributed to aromatic stacking interactions in nucleic acid complexes (*23*, *34*). In the case of tryptophan, charge-transfer character in the triplet state of a stacked complex is thought to contribute to an unusually large reduction of the zfs $D$ parameter. Charge-transfer involvement in the triplet state of stacked or intercalated DAPI complexes with nucleic acids probably is of lesser importance because of its lower energy relative to tryptophan. Intercalation of DAPI places it in a more polarizable environment than the aqueous solvent, and a redshift results mainly from London dispersion forces. Reduction of the zfs also is expected due to expansion of the electron orbitals in a polarizable environment. Binding of DAPI in the minor groove, on the other hand, produces a blueshift in the phosphorescence and a smaller reduction of the zfs. The reduction of the zfs is ascribed to increased

polarizability of the groove environment. The accompanying blueshift of the phosphorescence probably results from specifically directed electric fields that lower the ground-state energy more than that of the triplet state.

*Triplet State Kinetics.* The sublevel decay rate constants of DAPI (Table 2) are considerably higher than those of the parent molecule, indole or tryptophan. In tryptophan, for instance, $k_x$, $k_y$, and $k_z$ are 0.31, 0.10, and 0.00 $s^{-1}$, respectively (*25*). The greatly increased decay rate constants of DAPI relative to tryptophan are the result of enhanced radiationless decay rates due to its lower triplet state energy as well as to a larger density of vibrational states contributed by the conjugated side chains (*35*−*37*). As with tryptophan, $k_z < k_x$, $k_y$, which is expected for $^3(\pi, \pi^*)$ states of planar aromatic molecules, based on selective spin−orbit coupling patterns (*38*, *39*). While $k_x \sim 3k_y$ in tryptophan, these quantities are more nearly comparable in DAPI and its DNA complexes (Table 2). As in tryptophan, $T_x$ is the most highly radiative sublevel of free DAPI and its DNA complexes, based on the values of the $k_i$, and the $r_{ix}$. The similarities between DAPI and indole triplet states suggest that the electron distributions are similar, aside from the added delocalization afforded by the 6-amidinium and 2-phenyl-4′-amidinium groups of DAPI.

It has been noted (*35*−*37*) that, in the absence of heavy atom effects, the radiative decay rate constants, $k_{av}^{r} = {}^1/_3\sum k_i^{r}$, of all aromatic hydrocarbon triplet states fall within the range 0.033−0.1 $s^{-1}$ and that the large variation in phosphorescence lifetimes may be attributed to differences in intersystem crossing rate constants, $k_{av}^{nr} = {}^1/_3\sum k_i^{nr}$. For a given C/H ratio, it is found empirically that $k_{av}^{nr}$ of aromatic hydrocarbons decreases exponentially with increasing triplet state energy (*36*, *37*). The determination of $k_{av}^{nr}$ requires knowledge of the phosphorescence decay constant, $k_{av} = {}^1/_3\sum k_i$, and its radiative quantum yield, $Q_r \equiv k_{av}^{r}/k_{av}$. The experimentally accessible phosphorescence quantum yield, $Q_p$, may be expressed as

$$Q_p = Q_{isc}Q_r \tag{1}$$

where $Q_{isc}$ is the quantum yield for intersystem crossing to the triplet from the excited singlet state, $S_1$. Introducing the fluorescence quantum yield, $Q_f$, we can write

$$Q_{isc} = 1 - Q_f - Q_{nr} \tag{2}$$

where $Q_{nr}$ is the quantum yield of all radiationless processes from $S_1$, excluding intersystem crossing. Using data available from MIDP measurements, $Q_r$ can be expressed as

$$Q_r = {}^1/_3 q_x k_x(1 + r_{yx} + r_{zx})/k_{av} \tag{3}$$

where $q_x = k_x^{r}/k_x$, and it is assumed that the temperature is sufficiently high that the triplet sublevels are equally populated. Substituting eq 2 and eq 3 into eq 1, we get

$$Q_p = {}^1/_3 q_x k_x(1 + r_{yx} + r_{zx})(1 - Q_f - Q_{nr})/k_{av} \tag{4}$$

Using $Q_p = 0.17$ and $Q_f = 0.72$ obtained for tryptophan at 77 K (*40*) and the sublevel kinetic and relative radiative parameters from the MIDP measurements (*25*), eq 4 becomes

$$(0.28 - Q_{nr})q_x = 0.20 \tag{5}$$

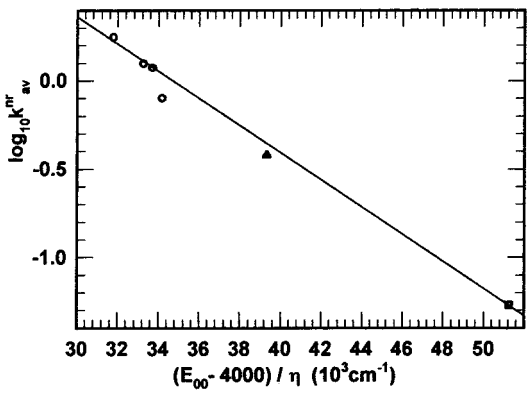


FIGURE 6: Siebrand plot (*36*) of the logarithm of the nonradiative decay constant, $k_{av}^{nr}$ versus $(E_{00}-4000)/\eta$ for the four DAPI samples investigated in this paper (○), naphthalene (▲), and tryptophan (□). The DAPI sample with the largest $E_{00}$ is the $[d(GGCCAATTGG)]_2$ complex. The least-squares regression has a slope of $-7.7 \times 10^{-5}$ cm and is calculated from tryptophan and the DAPI samples excluding the $[d(GGCCAATTGG)]_2$ complex.

Equation 5 requires that $Q_{nr} \leq 0.08$. At 77 K, $Q_{nr}$ represents mainly internal conversion, which is expected to be inefficient owing to the large $S_1-S_0$ energy gap of tryptophan. Thus, we will for the moment assume that $Q_{nr} \approx 0$, whereupon from eq 5 $q_x \approx 0.71$. It follows from eq 3 using the MIDP data for tryptophan (*25*) that $Q_r \approx 0.60$, $k_{av}^{r} \approx 0.082$ $s^{-1}$, and $k_{av}^{nr} \approx 0.054$ $s^{-1}$. (If $Q_{nr} \approx 0.08$ is assumed, we find that $Q_r \approx 0.85$, $k_{av}^{r} \approx 0.116$ $s^{-1}$, and $k_{av}^{nr} \approx 0.020$ $s^{-1}$. This radiative rate constant is beyond the range normally encountered for aromatic hydrocarbons, and the corresponding value of $k_{av}^{nr}$ (near that of benzene) is smaller than is found for nondeuterated triplet states of comparable energy (*35*−*37*). The parameters obtained from $Q_{nr} \approx 0$ are in good agreement with other molecules, and we will proceed using this assumption.)

In contrast with tryptophan, $k_{av}$ for DAPI is an order of magnitude larger and must be dominated by $k_{av}^{nr}$. If we assume that $k_{av}^{r}$ is the same as for tryptophan, the values of $k_{av}^{nr}$ of DAPI, the DAPI−$[d(CGACGTCG)]_2$ complex, the DAPI−$[d(GGCCAATTGG)]_2$ complex, and the DAPI−phosphate complex (monitored at 547 nm) are 1.18, 1.25, 0.80, and 1.77 $s^{-1}$, respectively. These rate constants increase with increasing phosphorescence redshift, as expected (*35*−*37*). Siebrand has shown (Figure 1, ref *36*) that, for a large number of aromatic hydrocarbon triplet states, log $k_{av}^{nr}$ decreases linearly with $(E_{00}-4000)/\eta$, where $E_{00}$ is in $cm^{-1}$ and $\eta = N_H/(N_H + N_C)$, $N_H$ and $N_C$ being the number of H atoms and C atoms in the molecule, respectively. Our data for tryptophan and DAPI fit well with the hydrocarbon data, if we assume the equivalence of N and C atoms in evaluating $\eta$. This assumption appears to be justified within Siebrand's theory provided that the N atoms do not carry lone pair electrons that are associated with low lying (n, $\pi^*$) states. The N atom of indole and those of DAPI do not carry lone pair electrons. When the data for tryptophan are included, each point, except that of the DAPI−$[d(GGCCAATTGG)]_2$ complex, falls accurately on a line of slope $-7.7 \times 10^{-5}$ cm on a Siebrand plot. Our data are presented in Figure 6, which also includes the naphthalene data point (*37*). The value of $k_{av}^{nr}$ of the DAPI−$[d(GGCCAATTGG)]_2$ complex is 20% lower than that predicted from the correlation of the other data in Figure 6, suggesting that intersystem crossing

is inhibited in this complex relative to the other DAPI systems studied. Thus, the N−H vibrations of the amidinium groups may contribute less efficiently to the Franck−Condon factors. It has been suggested that the amidinium groups are twisted in this structure and are involved in hydrogen bonding with guanine $NH_2$ groups (*20*). Their contribution to vibrational overlap may thus be inhibited, reducing $k_{av}^{nr}$.

## SUMMARY

Phosphorescence and ODMR spectroscopy are employed to characterize the phosphorescent state of DAPI and its complexes with phosphate, $[d(CGACGTCG)]_2$, and $[d(GGCCAATTGG)]_2$. DAPI is known to intercalate between GC base pairs of the former oligonucleotide and bind into the minor groove of the latter. The triplet state of DAPI, which contains an indole chromophore, has a lower energy than indole, and the zfs is reduced considerably; both effects are ascribed to increased delocalization of the $^3(\pi, \pi^*)$ state wave function due to conjugation with the 2-phenyl-4′-amidinium and 6-amidinium substituents. The ratio, $E/D$, although large, is reduced in DAPI relative to indole, probably another result of electron delocalization into the substituent groups. Binding to $[d(CGACGTCG)]_2$ induces a redshift in the phosphorescence of DAPI, while binding to the minor grove of $[d(GGCCAATTGG)]_2$ brings about a blueshift. The largest redshift of the complexes investigated results from binding to phosphate. Minor reductions of the zfs result from oligonucleotide binding (the effect of intercalation being larger than groove binding); a much larger reduction of the zfs is induced by phosphate binding and is ascribed to increased electron delocalization in the complex. As in indole, the largest decay rate constants are assigned to the in-plane sublevels $T_x$ and $T_y$, but the overall decay constant $k_{av}$ is larger by an order of magnitude than that of indole or tryptophan. This observation is in accord with the recognized dependence of the intersystem crossing rate constant to the ground state ($k_{av}^{nr}$) on the triplet state energy (*35*−*37*). For DAPI, each of its complexes (except the groove complex with $[d(GGCCAATTGG)]_2$), and tryptophan, log $k_{av}^{nr}$ plots linearly on a Siebrand plot (*36*). These data are in general agreement with rate data compiled for a large number of aromatic hydrocarbons (*35*−*37*). The radiationless decay constant of the DAPI−$[d(GGCCAATTGG)]_2$ complex is ca. 20% smaller than predicted by this correlation and may be the result of nonplanarity of the amidinium groups and their hydrogen bonding to guanine that is associated with the groove-binding mode (*20*). On the basis of these preliminary results, we suggest that intercalation and groove binding of DAPI may be distinguished by their opposite effects on the triplet state energy and lifetime.

## REFERENCES


1. Waring, M. J. (1981) in *The Molecular Basis of Antibiotic Action* (Gale, E. F., Cundiffe, E., Reynolds, P. E., Richmond, M. H., and Waring, M. J., Eds.) 2nd ed, p 287, Wiley, New York.
2. Haseltine, W. A. (1989) *JAIDS, J. Acquired Immune Defic. Syndr. 2*, 311−334.
3. Bresloff, M. J., and Crothers, D. M. (1981) *Biochemistry 20*, 3547−3553.
4. Nelson, J. W., and Tinoco, I., Jr. (1984) *Biopolymers 23*, 213−233.
5. Zimmer, C., and Wähnert, U. (1986) *Prog. Biophys. Mol. Biol. 47*, 31−112.
6. Pullman, B. (1983) *J. Biomol. Struct. Dyn. 1*, 773−794.
7. Dann, O., Bergen, G., Demant, E., and Voltz, G. (1971) *Justus Liebigs Ann. Chem. 749*, 68−89.
8. Straney, D. C., and Crothers, D. M. (1987) *Biochemistry 26*, 1987−1995.
9. Störl, K., Störl, J., Zimmer, C., and Lown, J. W. (1993) *FEBS Lett. 317*, 157−162.
10. Welch, J. J., Rausher, F. J., III, and Beerman, T. A. (1994) *J. Biol. Chem. 269*, 31051−31058.
11. Kapuchinski, J., and Szer, W. (1979) *Nucleic Acids Res. 6*, 3519−3534.
12. Williamson, D. H., and Fennel, D. J. (1975) *Methods Cell Biol. 12*, 335−351.
13. Cavatorta, P., Masotti, L., and Szabo, A. G. (1985) *Biophys. Chem. 22*, 11−16.
14. Kubista, M., Akerman, B., and Nordén, B. (1987) *Biochemistry 26*, 4545−4553.
15. Dervan, P. B. (1986) *Science 232*, 464−471.
16. Wilson, W. D., Tanious, F. A., Barton, H. J., Strekowski, L., and Boykin, D. W. (1989) *J. Am. Chem. Soc. 111*, 5008−5010.
17. Trotta, E., D'Ambrosio, E., Ravagnan, G., and Paci, M. (1995) *Nucleic Acids Res. 23*, 1333−1340.
18. Trotta, E., D'Ambrosio, E., Ravagnan, G., and Paci, M. (1996) *J. Biol. Chem. 271*, 27608−27614.
19. Tanious, F. A., Veal, J. M., Buczak, H., Ratmeyer, L., and Wilson, W. D. (1992) *Biochemistry 31*, 3103−3112.
20. Vlieghe, D., Sponer, J., and Van Meervelt, L. (1999) *Biochemistry 38*, 16443−16451.
21. Kwiram, A. L. (1982) in *Triplet State ODMR Spectroscopy* (Clarke, R. H., Ed.), pp 427−478, John Wiley and Sons, New York.
22. Ozarowski, A., Barry, J. K., Matthews, K. S., and Maki, A. H. (1999) *Biochemistry 38*, 6715−6722.
23. Maki, A. H., Ozarowski, A., Misra, A. Urbaneja, M. A., and Casas-Finet, J. R. (2001) *Biochemistry 40*, 1403−1412.
24. Wu, J. Q., Ozarowski, A., and Maki, A. H. (1996) *J. Magn. Reson., Ser. A 119*, 82−89.
25. Ozarowski, A., Wu, J. Q., and Maki, A. H. (1996) *J. Magn. Reson., Ser. A 121*, 178−186.
26. Wu, J. Q., Ozarowski, A., Davis, S. K., and Maki, A. H. (1996) *J. Phys. Chem. 100*, 11496−11503.
27. Ozarowski, A., and Maki, A. H. (2000) *J. Phys. Chem. B 104*, 1122−1127.
28. McGlynn, S. P., Azumi, T., and Kinoshita, M. (1969) *Molecular Spectroscopy of the Triplet State*, Prentice-Hall, Englewood Cliffs, NJ.
29. Smith, C., and Maki, A. H. (1993) *J. Phys. Chem. 97*, 997−1003.
30. Antheunis, D. A., Schmidt, J., and van der Waals, J. H. (1970) *Chem. Phys. Lett. 6*, 255−258.
31. Zuclich, J., von Schütz, J. U., and Maki, A. H. (1974) *J. Am. Chem. Soc. 96*, 710−714.
32. Hahn, D. K., and Callis, P. R. (1997) *J. Phys. Chem. A 101*, 2682−2691.
33. Ozarowski, A., Wu, J. Q., and Maki, A. H. (1998) *FEBS Lett. 422*, 52−56.
34. Wu, J. Q., Ozarowski, A., Maki, A. H., Urbaneja, M. A., Henderson, L. E., and Casas-Finet, J. R. (1997) *Biochemistry 36*, 12506−12518.
35. Robinson, G. W., and Frosch, R. P. (1963) *J. Chem. Phys. 38*, 1187−1203.
36. Siebrand, W. (1966) *J. Chem. Phys. 44*, *4055*−*4057*.
37. Siebrand, W. (1967) *J. Chem. Phys. 46*, 440−447; *47*, 2411−2422.
38. McClure, D. S. (1949) *J. Chem. Phys. 17*, 665−666.
39. Weissman, S. I. (1950) *J. Chem. Phys. 18*, 232−233.
40. Bishai, F., Kuntz, E., and Augenstein, L. (1967) *Biochim. Biophys. Acta 140*, 381−394.


BI020124J